



# Benchmarking of Industrial Synthetic Graphite Grades, Carbon Felt, and Carbon Cloth as Cost-Efficient Bioanode Materials for Domestic Wastewater Fed Microbial Electrolysis Cells

## OPEN ACCESS

Emma Roubaud<sup>1\*</sup>, Rémy Lacroix<sup>2</sup>, Serge Da Silva<sup>2</sup>, Luc Etcheverry<sup>1</sup>, Alain Bergel<sup>1</sup>, Régine Basséguy<sup>1</sup> and Benjamin Erable<sup>1</sup>

### Edited by:

Uwe Schröder,  
Technische Universität  
Braunschweig, Germany

### Reviewed by:

Feng Zhao,  
Institute of Urban Environment  
(CAS), China  
Robert Keith Brown,  
Technische Universität  
Braunschweig, Germany

### \*Correspondence:

Emma Roubaud  
emma.roubaud@ensiacet.fr

### Specialty section:

This article was submitted to  
Bioenergy and Biofuels,  
a section of the journal  
Frontiers in Energy Research

**Received:** 19 June 2019

**Accepted:** 19 September 2019

**Published:** 09 October 2019

### Citation:

Roubaud E, Lacroix R, Da Silva S, Etcheverry L, Bergel A, Basséguy R and Erable B (2019) Benchmarking of Industrial Synthetic Graphite Grades, Carbon Felt, and Carbon Cloth as Cost-Efficient Bioanode Materials for Domestic Wastewater Fed Microbial Electrolysis Cells. *Front. Energy Res.* 7:106. doi: 10.3389/fenrg.2019.00106

<sup>1</sup> Laboratoire de Génie Chimique, Université de Toulouse, CNRS, INPT, UPS, Toulouse, France, <sup>2</sup> 6T-MIC Ingénieries, Castanet-Tolosan, France

Anode material selection is crucial when it comes to building up-scaled microbial electrolysis cells (MEC), as it has a huge influence on the achievable current density and account for a large part of the MEC total investment cost. Graphite is a material that is perfectly suited to the creation of up-scaled bioanodes as it is conductive, chemically stable, biocompatible, and relatively cheap but there are a very large number of commercially available grades of industrial graphite. In this study, five grades of industrial synthetic graphite (named G1–G5) were bench tested to select the most suitable grade for future development of 3D bioanode for domestic wastewater (dWW) fed MEC application. The five grades of graphite have been selected with similar physico-chemical and surface properties (electrical resistivity, surface roughness, and hydrophobicity) theoretically appropriate for EA biofilm development. Nevertheless, significant current density disparities were observed with the five graphite grades, which can certainly be explained by the fabrication procedures of the respective material grades. With the graphite grade giving the most efficient anodes (G3), an average steady state current density of 2.3 A/m<sup>2</sup> was produced, outperforming the other grades by at least 15%. Even though all graphites had very close physico-chemical characteristics, the grade had a clear significant influence on the current densities produced. G3 graphite was finally compared to carbon felt (CF) and carbon cloth (CC) both in terms of bio-electrochemical current production and bacterial communities colonizing electrodes. G3 bioanodes outperformed CF and CC bioanodes by 50% in term of steady state current density. Biofilms microbial population analysis showed that the *Geobacter* species was present at 82% on G3 bioanodes, 39% on CF bioanodes, and 61% on CC bioanodes when it was only present at 0.06% in the activated sludge used as inoculum. This significant difference

in bacterial enrichment could come from the huge gap between materials resistivity, as graphite resistivity is 200-fold lower than CF and CC resistivities. The strongly hydrophilic surface of G3 graphite was also certainly beneficial for biofilm development compared to the hydrophobic surfaces of CF and CC.

**Keywords:** anodic biofilm, microbial population analysis, MEC, wastewater treatment, electrode material benchmarking, hydrogen

## INTRODUCTION

Microbial electrolysis cells (MEC) allow combining wastewater treatment and production of hydrogen at low cost. They combine the ability of electroactive (EA) bacteria to oxidize organic matter, using the anode as an electron acceptor, with the hydrogen evolution reaction at the cathode (Liu et al., 2004; Gil-Carrera et al., 2013). The valorization of this hydrogen as an energy source reduces the environmental impact associated with the chemical oxygen demand (COD) removal during wastewater treatment (Gude, 2016).

The up-scaling of MEC reactors fed with real domestic wastewater (dWW) is a challenge that requires optimization of reactor geometry (Heidrich et al., 2013; Kadier et al., 2014), electrolyte composition (Roubaud et al., 2018), electrode material and design (Wei et al., 2011; Hou et al., 2015; Xie et al., 2015), microbial consortia management, inoculation strategy (Bridier et al., 2015; Kitching et al., 2017), and operating conditions (temperature, hydraulic retention time, initial COD-load, cell voltage) (Nam et al., 2014; Pannell et al., 2016). MEC up-scaling must also consider financial viability to make the MEC technology to be economically competitive with other hydrogen production and wastewater treatment processes. This first involves reducing the construction costs of MECs as much as possible without affecting their performance. Aiken et al. (2019) recently established that anodic materials represent up to 75% of the total material cost of a MEC at an industrial scale. In this context, the anode material must be carefully chosen to minimize its impact on investment costs and ensure its durability to guarantee a sustainable investment for the exploitation of the technology in the long term.

Graphite, in addition to offering many proven advantages as an anode material in MEC (conductive, chemically stable, biocompatible...), has a relatively low price (Wei et al., 2011; Zhou et al., 2011) and a mechanical resistance over time that has already proven to be successful in many industrial fields other than MECs (metallurgical industry, electrical and electronic industries, aerospace...). In addition, graphite can be machined and assembled to create three-dimensional geometries of customized electrodes, with a controlled pore size (Chong et al., 2019), which could offer compact electrodes with maximized oxidation kinetics in domestic wastewater in the near future.

There are two types of graphite used in the industry: natural graphite and synthetic or artificial graphite. Natural graphite is a natural element mainly used as a lubricant, carbon additive, and pencil lead. Synthetic graphite is a composite material synthesized from petroleum used in a

variety of applications requiring properties superior to those of natural graphite. The problem is that there are several grades or qualities of synthetic graphite available on the market whose physical, chemical, and surface characteristics depend largely on their production process: extrusion, vibration molding, compression molding, and isostatic molding. Their price generally varies according to their mechanical strength and premium graphite grades can easily be twice as expensive as low cost graphite grades.

Despite the tremendous amount of work relating to the use of graphite electrodes in MECs and even more widely in all BESs, no one has yet taken a closer look at the consequences of the use of different synthetic graphite grades on the formation and performance of anode EA biofilms. This is what we investigated in this study, by comparing five industrial synthetic grades of graphite plates selected *a priori* to have similar physico-chemical parameters in terms of electrical resistivity, surface roughness and hydrophobicity, probably conditioned by material elaboration protocols. In addition, all five graphite grades were theoretically optimal for biofilm development since they displayed low electrical resistivity, hydrophilic surfaces, and average roughness above 0.8  $\mu\text{m}$  (Flint et al., 2000; Santoro et al., 2014).

Bioanodes were formed with each graphite grade in real dWW collected from a sewage treatment plant with a standardized bio-electrochemical protocol i.e., fixed electrode potential and constant COD concentration. To interpret differences in the bio-electrochemical behavior, materials surface analysis was performed by SEM observation, and microbial communities from biofilms formed on the various electrodes were analyzed by 16S rRNA gene amplicon pyrosequencing. In the end, one graphite grade was selected by taking into account the steady state current densities produced by the bioanodes as well as the graphite price and mechanical resistance. The bio-electrochemical performance of the selected graphite grade were then compared with two other materials commonly used as bioanode supports: carbon cloth (CC) and carbon felt (CF) (Liu et al., 2010; Wei et al., 2011).

## MATERIALS AND METHODS

### Inoculum and dWW Supply

dWW from a local sewage treatment plant (Castanet-Tolosan, France) was used as electrolyte aqueous medium and COD source for the bioanodes. Activated sludge (AS) obtained from the same treatment plant was used as inoculum (5% v/v of AS in dWW).

The dWW COD was measured with commercial cuvette tests (LCK 514, Hach). For soluble COD, membrane filtration (0.2  $\mu\text{m}$ , Minisart® PES, Sartorius) was performed before measurement.

Before being used as feeding medium, dWW was hydrolyzed for 7 days in hermetically sealed 2 L glass bottles flushed with  $\text{N}_2$  for 15 min at a flow rate of 10 mL/s. This hydrolysis step allows increasing the soluble COD concentration that will stay constant during 7 supplementary days (see **Supplementary Figure 1**). The average soluble COD of hydrolyzed dWW is 380 mg/L and average total COD is 800 mg/L.

## Bio-Electrochemical Setup and Protocol

Bioanodes were formed on five different grades of graphite plate (Graphitech, France) labeled G1–G5 in this study. **Table 1** displays the characteristics given by the supplier for each grade.

For the graphite grades comparison experiments, the electrodes were prepared by coating  $2 \times 2 \times 0.5$  cm graphite plates with insulating varnish and drilling a hole of 1 cm diameter in the center of the electrode (see **Supplementary Figure 2**), so that only the surface inside the hole (surface area = 1.57  $\text{cm}^2$ ) was electroactive. This has made possible to exclude the influence of any surface residue from the manufacturing process and ensured comparable surface states between the five grades of graphite.

Bioanodes were also formed on carbon felt (CF, RVG 4000, Mersen, France), and carbon cloth (CC, Paxitech, France) and the flat surface of the G3 graphite for comparison. In this case, the electrodes were  $2 \times 1$  cm pieces of each material.

All the experiments were conducted with 3-electrode set-ups. Working electrodes (graphite, CF, or CF) were connected to a titanium rod that served as the current collector. The counter electrode was a  $15 \times 3$  cm 316 L stainless steel grid arranged in a circular shape around the working electrode. The grid was connected to a 316 L SS wire that served as the current collector. The reference electrode was a saturated calomel electrode (SCE, Radiometer Analytical +0.24 V/SHE) and was placed as close as possible to the working electrode (around 2 cm).

The protocol was defined in order to perform strictly identical comparative tests with the different anode materials. The 600 mL bio-electrochemical reactors were initially filled with a mix of dWW and 5% v/v of AS and were continuously sparged with nitrogen gas flux (5 mL/s). The anodes were polarized at  $-0.1$  V/SCE and the current was recorded every 10 min (Chronoamperometry, CA). Cyclic voltammetry (CV) was recorded at 1 mV/s in the  $-0.5$  to  $+0.2$  V/SCE range at the beginning and end of the experiments.

**TABLE 1** | Characteristics of industrial synthetic graphite grades, given by the supplier.

	G1	G2	G3	G4	G5
Electric resistivity ( $\mu\Omega\cdot\text{m}$ )	10.4	8.4	12.0	14.0	13.0
Mechanical strength (compressive strength) (MPa)	32	37	90	150	170
Price/ $\text{m}^2$ (€)	501.2	507.9	533.1	679.8	1090.9

The reactors spent 10 days in batch mode. Then, each reactor was connected to a 2 L tank of dWW that had previously been hydrolyzed for 7 days to reach a stable soluble COD concentration (see section Inoculum and dWW Supply). Then, the reactors were operated in recirculating mode for 14 more days thanks to a peristaltic pump with a flow rate of 1.5 mL/min (hydraulic retention time = 6.7 h). The tubes used for the hydraulic recirculation of dWW were oxygen-proof (Tygon, Masterflex).

The dWW tank was renewed with fresh hydrolyzed dWW every 7 days with the aim of maintaining a high and constant soluble COD concentration. The amount of soluble COD consumed by the bioanode was very low thanks to the small size of the bioanode. Here the analytical system was not designed to obtain high COD degradation ratios, but to maintain COD as constant as possible in order to compare the different electrode materials in identical and stable conditions.

## Materials Surface Analysis

### Scanning Electron Microscopy (SEM)

Biofilms were fixed on the electrode in phosphate buffer (400 mM, pH = 7.4) with 4% glutaraldehyde for 20 min. They were rinsed in phosphate buffer containing saccharose (0.4 M) and dehydrated by immersion in increasing concentrations of acetone (50, 70, 100%), then in acetone and hexamethyldisilazane (50:50), and in 100% hexamethyldisilazane (HMDS). The last batch of HMDS was air-dried until complete evaporation. Surfaces were observed with a LEO 435 VP scanning electron microscope.

For non-colonized anode materials, no treatment was performed before SEM observation.

### Surface Roughness

Experimental measurements were performed on each grade of graphite. Surface roughness was measured with an optical microscope (S-Neox, Sensofar) with the focus variation method. This method combines the small focus depth of an optical system with vertical scanning to provide topographical information from the variation of focus<sup>1</sup>.

Two roughness parameters were measured: the spatial arithmetic average height ( $S_a$ ) and the spatial kurtosis ( $S_{ku}$ ), which indicate if the peaks and valleys are smooth (low  $S_{ku}$ ) or steep (high  $S_{ku}$ ). The measurements were performed on 4  $\text{mm}^2$  surfaces and 5 different locations on the electrode.

### Water Contact Angle

Water contact angle measurements were performed using a tensiometer (DSA 100, Krüss) with the captive bubble method. An air bubble was produced on the underside of a graphite plate which was immersed in water<sup>2</sup> (Drop Shape Analyzer—DSA100). The ADVANCE software was used to measure the

<sup>1</sup>Focus-Variation|Alicona—High-resolution optical 3D measurement Available online at: <https://www.alicon.com/focus-variation/> (accessed August 29, 2018).

<sup>2</sup>Drop Shape Analyzer—DSA100 Available online at: <https://www.kruss-scientific.com/products/contact-angle/dsa100/drop-shape-analyzer-dsa100/> (accessed August 29, 2018).

resulting contact angle. The measurements were performed on 5 different locations for each grade of graphite.

## Bacterial Community Analysis

The bioanodes were put in plastic tubes with 50 mL of phosphate buffer and placed in an ultrasonic bath at 80 W for 30 min to detach the biofilm. Two 50 mL tubes were also prepared with dWW and AS samples.

The tubes were centrifuged for 15 min at 4,600 g at 6°C. The supernatant was discarded and a DNA extraction kit (DNeasy PowerBiofilm, Qiagen) was used on the pellets according to the manufacturer's recommendations. Full pellets (~0.03 g) were used for the biofilm samples and ~0.20 g pellets for the AS and dWW samples. The DNA concentrations were checked with absorbance at 260 nm as well as the possible contamination by protein and humic acid with absorbance at 280 and 230 nm, respectively. The DNA samples were sent to the Research and Testing Laboratory (RTL, Texas, USA) where the DNA were amplified by PCR and sequenced with the bacterial primers 28F (5'-GAG TTT GAT YMT GGC TC-3') and 519R (5'-GWA TTA CCG CGG CKG CTG-3') according to RTL protocols<sup>3</sup> (RTLGenomics). Subsequent data analyses with the DNA quality, DNA sequence alignment, clustering in operational taxonomic and the assignment were also performed by RTL according to their protocol.

## RESULTS AND DISCUSSION

### Physico-Chemical Surface Properties of the Different Grades of Graphite

Physico-chemical properties of the bioanode material such as surface roughness, hydrophobicity, and electrical resistance affect the formation of electroactive (EA) biofilm on its surface (Santoro et al., 2014).

#### Surface Roughness

The average roughness ( $S_a$ ) of graphite surface was between 1.3 and 4.4  $\mu\text{m}$  (Table 2). In general, surfaces with  $S_a$  lower than 0.8  $\mu\text{m}$  are considered as "hygienic" surface and are not suitable for microbial growth (Flint et al., 2000). Moreover,  $S_a$  values in the range of 1–10  $\mu\text{m}$  are ideal for biofilm adhesion (Pons et al., 2011; Kano et al., 2012; Santoro et al., 2014; Champigneux et al., 2018). Indeed, bacteria particularly prefer rough areas and surface deformations, which size range is of the same order of magnitude as the size of the bacteria, i.e., in the order of a few micrometers. The surface roughness measurements indicate that all selected graphite grades present a suitable surface roughness for biofilm development.

The kurtosis roughness ( $S_{ku}$ ) represents the sharpness of the surface<sup>4</sup>.

<sup>3</sup>RTLGenomics. Available online at: <https://rtlgenomics.com/> (accessed April 8, 2019).

<sup>4</sup> $S_{ku}$  (Kurtosis)/Area Roughness Parameters[Introduction To Roughness|KEYENCE America. Available online at: <https://www.keyence.com/ss/products/microscope/roughness/surface/sku-kurtosis.jsp> (accessed March 19, 2019).

- if  $S_{ku} < 3$ : Height distribution is skewed above the mean plane.
- if  $S_{ku} = 3$ : Height distribution is normal (sharp portions and indented portions co-exist).
- if  $S_{ku} > 3$ : Height distribution is spiked (high peaks, large valleys).

Characklis (2009) has stated that surface roughness elements, such as peaks and valleys, can provide "shelter" from shear forces for bacteria and increase convective mass transport near the surface. Thus,  $S_{ku}$  is an interesting parameter to assess if a surface is favorable for bacterial adhesion.

Graphite surfaces can be divided in two categories: graphites with spiked surfaces (G1, G2, and G3;  $S_{ku} \gg 3$ ) and graphites with smooth surfaces (G4 and G5;  $S_{ku}$  close to 3). Biofilm bacteria growing on G4 and G5 would be less protected from shear forces, leading to more bacterial detachment with those graphite grades when compared with G1, G2, and G3 (Picioreanu et al., 2001).

#### Surface Hydrophobicity

Water contact angle measurements showed that all five graphite grades have hydrophilic surfaces (contact angle  $\ll 90^\circ$ ). Contact angle values range from 33 to 36°, which means there is no significant difference between graphite grades hydrophobicity (Table 3).

Santoro et al. (2014) have compared the effect of hydrophilic and hydrophobic surfaces on bacterial attachment, current, and power output in microbial fuel cells. Bioanodes formed on hydrophilic surfaces showed the shortest start-up time, the highest current, and power densities and the fastest electron transfer rates among the materials investigated. Also, Guo et al. (2013) demonstrated that positively charged and hydrophilic surfaces were more selective to EA microbes (e.g., *Geobacter*) and more conducive for EA biofilm formation.

As a conclusion, all five grades of graphite have strongly hydrophilic surfaces, which would be beneficial for bacterial attachment according to the literature. However, the difference between the measured contact angles for the five grades of graphite is slight, material hydrophobicity will not be a differentiation factor for the bioanode performance.

#### Electrical Resistivity

Graphite resistivity was on average 11.6  $\mu\Omega\cdot\text{m}$  for the 5 graphite grades (Table 1). These values are significantly higher than that of

**TABLE 2 |** Surfaces roughness ( $S_a$  and  $S_{ku}$ ) experimentally measured on graphite grades.

		G1	G2	G3	G4	G5
Surface roughness	$S_a$ ( $\mu\text{m}$ )	4.4 ± 0.5	4.2 ± 0.2	1.9 ± 0.1	2.6 ± 0.1	1.3 ± 0.1
	$S_{ku}$	48 ± 13	26 ± 2	17 ± 7	3.8 ± 0.1	4.9 ± 0.3

**TABLE 3 |** Water contact angle on graphite grades, measured experimentally.

	G1	G2	G3	G4	G5
Contact angle	35 ± 5°	35 ± 1°	36 ± 2°	33 ± 2°	34 ± 2°

metallic materials such as stainless steel ( $\sim 0.7 \mu\Omega\cdot\text{m}$ ) (Peckner and Bernstein, 1977) or copper ( $0.02 \mu\Omega\cdot\text{m}$ ). Despite their low resistivity, metallic materials are not an obvious choice as bioanode materials since they do not always fulfill the other criteria required (chemical stability and bio-compatibility). Nevertheless, remarkable current densities were obtained on stainless steel electrodes in MFC inoculated with compost leachate (Pocaznoi et al., 2012a; Ketep et al., 2014) or on copper and silver electrodes inoculated with dWW (Baudler et al., 2015).

For Wang et al. (2013), solid graphite resistivity is low enough and its impact on the ohmic losses of BES cells is negligible, even in up-scaled reactors, which is not the case for granular or fibrous carbon materials (Baudler et al., 2015). Graphite is about 200 times less resistant than CF and CC (González-García et al., 1999) which are widely used as bioanode materials and with which remarkable current densities were still obtained (Cercado-Quezada et al., 2013).

The resistivity range of materials used as EA biofilm support in the literature is truly broad. The resistivity range of the 5 graphite grades considered here (from 8.4 to  $14.0 \mu\Omega\cdot\text{m}$ ) is narrow enough not to affect current densities.

## Comparison of Industrial Grades of Graphite as Bioanode Material Bio-Electrochemical Experiments

The five grades of graphite were tested to generate bioanodes from real dWW (protocol described in section Materials Surface Analysis). As discussed above, all five grades have suitable physico-chemical properties to allow biofilm growth on the surface: average surface roughness above  $0.8 \mu\text{m}$ , hydrophilic surface and low electrical resistivity.

The current densities recorded during the 24 days of the CA are displayed on **Figure 1**.

In the initial batch period, current rise happened in the first 3–4 days for graphite grades G2, G3, and G4 as well as one G1 duplicate. For the other G1 and both G5 duplicates, the current rise happened later, after the 5th day. Maximum current density was reached during the batch period for G2 and G4 and during the recirculation period for G1, G3, and G5. Setting up the recirculation had little effect for G2 and G4 but triggered a current growth for G1, G3, and G5. During the recirculation period, with a stationary concentration of  $380 \text{ mg}_{\text{solubleCOD}}/\text{L}$ , steady state current was obtained from day 10 for G4, from day 11 for G1 and G2, from day 13 for G3, and from day 14 for G5.

As the current densities achieved stability at different points in time for each graphite grade, the steady state current density value was evaluated on both duplicates by averaging the current density values recorded from the first day of current generation stability to the end of the experiment (**Table 4**).

Steady state current densities ranged from 1.1 to  $2.3 \text{ A}/\text{m}^2$ . The lowest was obtained with G5, then G1, G4, G2, and the highest was obtained with G3. The steady state current generated by the G3 based electrodes was 15% higher than G2 (second best performing graphite

grade) and 110% higher than G5 (least performing graphite grade).

To sum up, efficient EA biofilms developed on the five graphite grades. Significant current densities disparities were observed from one graphite grade to another despite them having similar hydrophilia and electrical resistance. The main differences between grades was the surface roughness ( $S_a$  and  $S_{ku}$ ) but no obvious correlation was found between roughness parameters and steady state current densities. In conclusion, even when the major physico-chemical parameters are restricted to narrow ranges, the grade of industrial graphites reveals here to affect significantly the current provided by the bioanodes formed on the different materials. It is strongly suspected that these differences are mainly related to the production processes of the material grades. Experimental tests remain consequently necessary to check the capability of industrial graphite materials to drive the formation of efficient bioanodes.

## Graphite Selection Considering Cost of Investment and Mechanical Strength

Apart from the physico-chemical characteristics of the materials, the investment cost of graphite is also an important indicator of the economic competitiveness of bioanodes applications.

In order to design an economically sustainable MEC, the anode material must be cheap and readily available. Wei et al. compared the bulk price for common electrode materials and stated that graphite was up to 50 times cheaper than CF or carbon fiber brushes (Wei et al., 2011).

Among the 5 grades of graphite tested, G1, G2, and G3 are the least expensive and are in the same range of price when G4 and G5 are significantly more expensive (up to twice as expensive for G5). Considering that anode materials account for 75% of an up-scaled MEC total material cost (Aiken et al., 2019), using a low-end graphite such as G1, G2, or G3 with a price twice as low as G5 would decrease up-scaled MECs investment costs by almost 40%. A case study about investment costs for the implementation of MECs in domestic wastewater treatment plants by Escapa et al. (2012) proposes a scenario in which a  $108,300 \text{ m}^2$  bioanode produces a current density of  $2.5 \text{ A}/\text{m}^2$ , which is the same order of magnitude of the average current densities produced by the G3 bioanodes. As an example, in this scenario, using an electrode material costing about  $50 \text{ €/m}^2$  instead of  $100 \text{ €/m}^2$  would reduce the anode material cost by about 5 million euros.

Considering steady state current density and price, G2 and G3 have the best price-performance ratio. The main difference between those two graphite grades is their production process, which influences their mechanical strength. G3 graphite is produced through isostatic pressure as opposed to G2 that is produced through extruding. The isostatic pressure technique allows producing graphite with higher mechanical strength, making G3 compressive strength almost 1.5 times higher than G2. Overall, G3 is the most suited graphite grade to use as bioanode material in the context of an up-scaled MEC as its performance/price ratio is excellent and its mechanic strength is the highest among all graphite grades in the same price range.

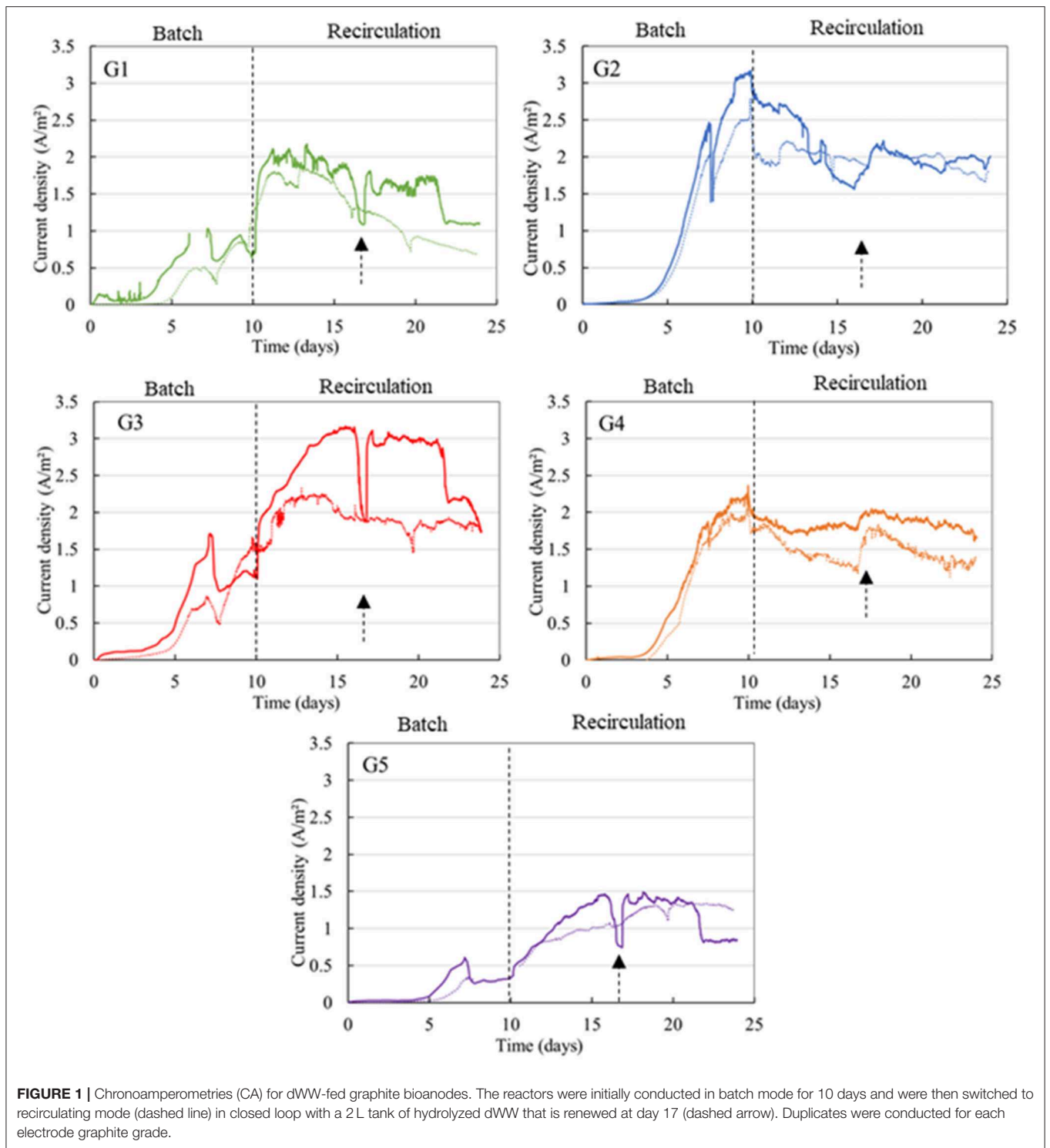


**FIGURE 1 |** Chronoamperometries (CA) for dWW-fed graphite bioanodes. The reactors were initially conducted in batch mode for 10 days and were then switched to recirculating mode (dashed line) in closed loop with a 2L tank of hydrolyzed dWW that is renewed at day 17 (dashed arrow). Duplicates were conducted for each electrode graphite grade.

**TABLE 4 |** Steady state current densities and maximal current densities obtained with the 5 grades of graphite.

	G1		G2		G3		G4		G5			
Steady state current density (A/m <sup>2</sup> )	Run 1	Run 2	1.7 ± 0.3	1.3 ± 0.4	2.0 ± 0.3	1.9 ± 0.2	2.8 ± 0.4	1.9 ± 0.2	1.8 ± 0.2	1.5 ± 0.2	1.2 ± 0.3	1.1 ± 0.2
	Mean value		1.5		2.0		2.3		1.6		1.1	

The current values are given for each run and the mean value is calculated on the line underneath.

## Comparison of the G3 Grade of Graphite With Classical CF and CC Electrodes Bio-Electrochemical Experiments

CF and CC are among the most commonly used anode materials in bioelectrochemical systems (Santoro et al., 2017; Yu et al., 2017) because they offer a porous 3-dimensional structures that can lead to efficient bioanodes in environments with low suspended solids and poor COD load. In order to validate the selection of G3 graphite grade, this material was compared to CC and CF in term of steady state current density. Bioanodes were formed in duplicates with G3 graphite plates, CF, and CC at the same time and using the same batch of AS and dWW to ensure strictly comparable results. The current densities recorded during the 24 days of the CA are displayed on **Figure 2** (left).

In the batch period, graphite and felt electrodes had similar behaviors with a current rise happening around the 5th–7th day. With the CC electrodes, no significant current rise was observed during the batch period.

When recirculation was started, the current kept rising for around 5 days with graphite and started to stabilize with CF. The current started to rise with CC. A steady state was achieved on the 13th day for graphite and CF and on the 18th day for CC. The current density value for the stationary phase was evaluated in the same way as in section Physico-Chemical Surface Properties of the Different Grades of Graphite. The values obtained are displayed in the **Table 5**. CF gave the most reproducible CAs, with an equal steady state current value on both runs (<3% difference between runs based on the average steady state current density value given in the **Table 5**). Difference between the two runs with the G3 graphite grade is 23%. CC was the less reproducible with 33% difference when steady state current density was reached.

The G3 graphite grade gave the highest steady state current with an average of 3.1 A/m<sup>2</sup>. It is about 50% higher than steady state current densities obtained with CF and CC, which were 2.0 and 2.1 A/m<sup>2</sup>, respectively.

When the steady state current was established on the different bioanodes (day 24), turnover CV were recorded with stable soluble COD concentrations (**Figure 2**, right). The shape of the turnover CV is characteristic of bioanodes oxidizing volatile fatty acids present in soluble COD (mainly acetate, formate, butyrate and propionate (Barker et al., 1999), at neutral pH (Pocaznoi et al., 2012b; Cercado-Quezada et al., 2013). The half-wave potentials are in the range of –0.4 to –0.3 V/SCE for G3 graphite, –0.22 V/SCE for CF, and in the range of –0.35 to –0.2 V/SCE for CC.

Current density showed a plateau value of 2.4 A/m<sup>2</sup> for CF, 3.2 A/m<sup>2</sup> for graphite, and 2.2 A/m<sup>2</sup> for CC, very similar to steady state current densities recorded on the CAs.

### Microbial Electrode Colonization

**Figure 3** displays the SEM observation of the 3 bioanode materials before and after biofilm colonization, i.e., at day 0 and after day 24 of the bioanode formation.

Before colonization (**Figure 3**, 1a), G3 graphite surface topography is not smooth and present some topographic peaks and valleys, in accordance with the roughness measurements

(**Table 2**). The CF structure seems quite open, with a fiber diameter of about 20 μm (**Figure 3**, 1b). Inter-fiber spaces are variable between 10 and 500 μm. The fiber diameter of CC is about 10 μm (half the size of CF fibers). The fibers are tightly woven which makes inter-fiber spaces difficult to evaluate. On a bacterial scale, cloth porosity is almost non-existent.

After 24 days, a continuous biofilm with homogeneous visual appearance has developed on the G3 graphite surface (**Figure 3**, 2a). This biofilm seemed thicker than those developed on CF and CC because no more peaks or valleys can be observed by SEM on the graphite surface. On CF, biofilm was mainly located on the external fibers and did not cover the whole surface of the fibers nor all the volume of porosity between the fibers (**Figure 3**, 2b). The biofilm established on the CC electrode had fully covered the surface area of the electrode (**Figure 3**, 3b). However, its thickness was estimated at only 15 μm, because visually the topography of the CC under the biofilm layer was still visible.

Overall, the biofilm colonization is important on the three materials, with however a seemingly smaller biofilm density on CF. This certainly explains why the current densities obtained are in the same range. Theoretically, CF has a higher specific surface area than CC and the G3 graphite. The current densities should consequently have been higher on this material. Nevertheless, the biofilm only developed on the external fibers and did not penetrate inside the felt. Felt did not perform better than 2D materials such as cloth or graphite in real dWW. The poor infiltration of EA biofilm into the macro porosity of CF has already been highlighted (Blanchet et al., 2016).

### Bacterial Population Ecology of EA Biofilms

Microbial population analysis was performed on the biofilms removed from the three types of electrodes as well as on dWW and AS used, respectively, as electrolyte and inoculum to form the bioanodes.

The three biofilms showed similar bacterial classes, with some variation in the relative abundance rate (**Figure 4**). On the one hand, the class of *Deltaproteobacteria* was systematically enriched in all biofilms formed on the electrodes (82% on G3 graphite, 39% on CF, and 61% on CC) regardless of the nature of the electrode material while this class of bacteria was only present at 0.06% in activated sludge and even not detected in dWW. On the other hand, a higher percentage of *Betaproteobacteria* is present on CF (11%) and CC (9%) than on graphite (<1%). This bacterial class is largely represented in AS and dWW but is depleted to the benefit of *Betaproteobacteria* on the graphite electrode.

For Mateo et al. (2018) biofilms grown on various carbon materials (carbon paper, carbon foam, and carbon cloth) showed the same microbial population. The performance gap between the electrodes came from the variation of specific surface area between the materials.

The proportion of *Deltaproteobacteria* in biofilms coincided well with the current density generated, i.e., the more efficient the bioanodes are, the higher the relative abundance of *Deltaproteobacteria*. At the family level, 99% of those *Deltaproteobacteria* belong to *Geobacteraceae*. Many studies conducted on bioanodes inoculated with soils, activated sludge or marine sediments come to the same conclusion that EA biofilms

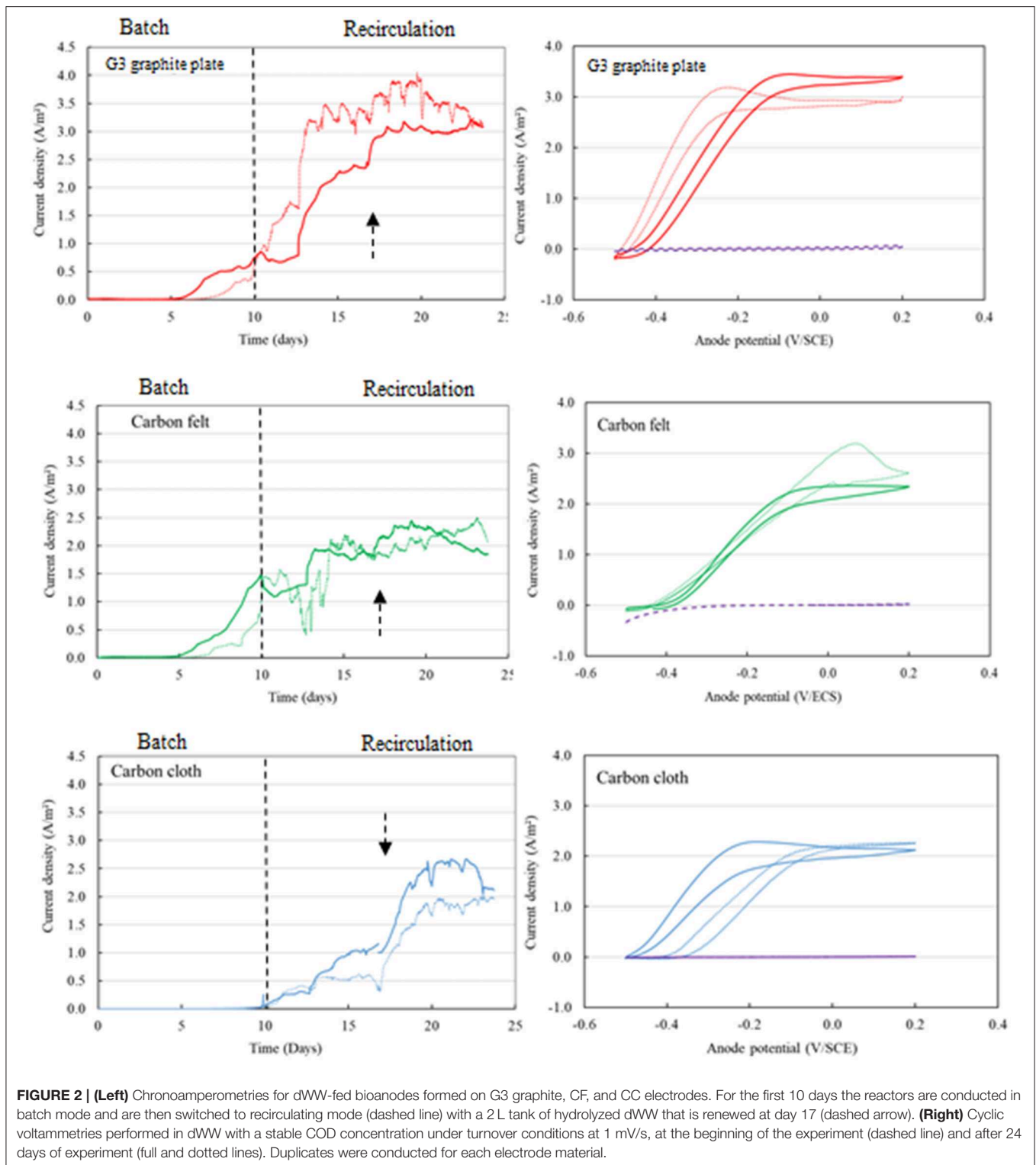


**FIGURE 2 | (Left)** Chronoamperometries for dWW-fed bioanodes formed on G3 graphite, CF, and CC electrodes. For the first 10 days the reactors are conducted in batch mode and are then switched to recirculating mode (dashed line) with a 2 L tank of hydrolyzed dWW that is renewed at day 17 (dashed arrow). **(Right)** Cyclic voltammograms performed in dWW with a stable COD concentration under turnover conditions at 1 mV/s, at the beginning of the experiment (dashed line) and after 24 days of experiment (full and dotted lines). Duplicates were conducted for each electrode material.

are especially enriched in species from the *Geobacteraceae* family (Bond et al., 2002; Cercado-Quezada et al., 2013; Blanchet et al., 2015). Among *Geobacteraceae*, some species have been isolated (*sulfureducens*, *metallireducens*, and others...)

(Koch and Harnisch, 2016), which are now used as model EA bacteria (Reguera et al., 2005; Kumar et al., 2016).

To conclude, G3 graphite out-performed the two other materials by 50% in term of steady state current density.

**TABLE 5** | Average current density obtained in steady state on CF, CC, and G3 graphite.

Steady state current density (A/m <sup>2</sup> )	G3 graphite		Felt		Cloth			
	Run 1	Run 2	2.7 ± 0.5	3.4 ± 0.2	2.0 ± 0.2	2.0 ± 0.3	2.4 ± 0.2	1.7 ± 0.2
	Average		3.1		2.0		2.1	

Given for each replicate and averaged on both replicates.

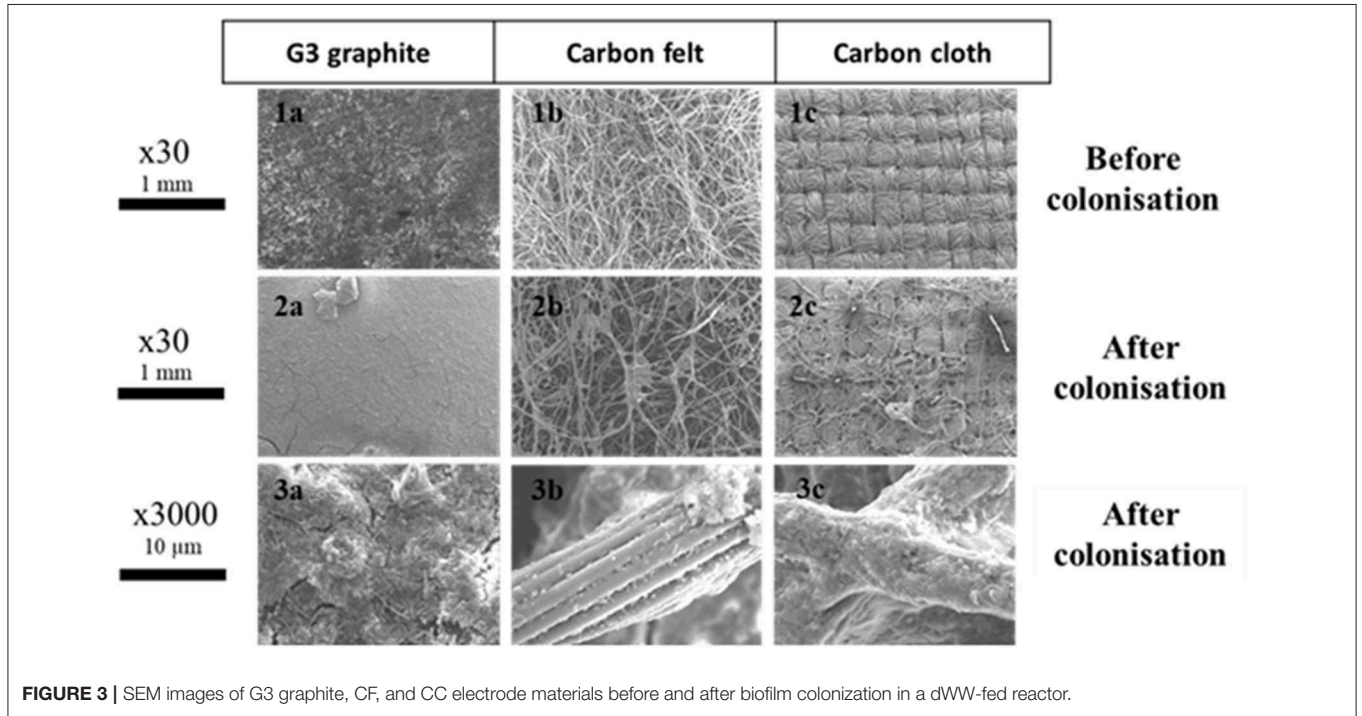


**FIGURE 3** | SEM images of G3 graphite, CF, and CC electrode materials before and after biofilm colonization in a dWW-fed reactor.

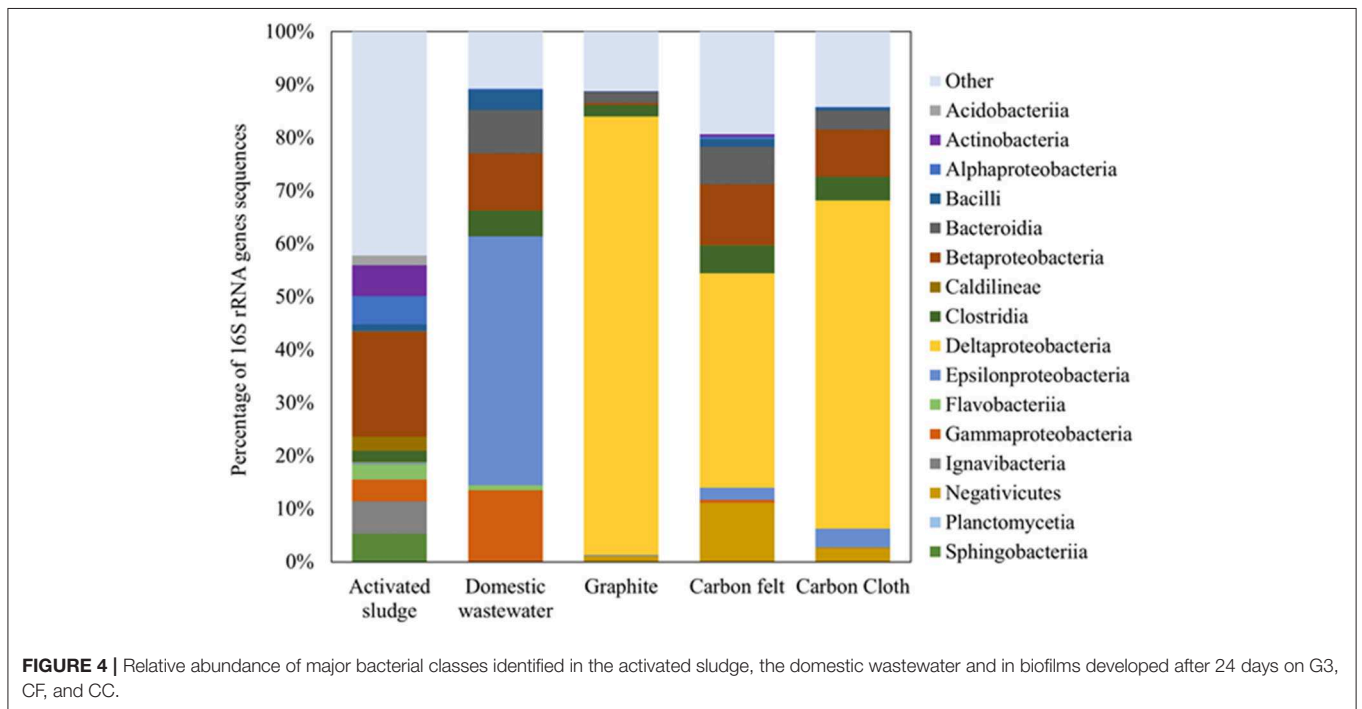


**FIGURE 4** | Relative abundance of major bacterial classes identified in the activated sludge, the domestic wastewater and in biofilms developed after 24 days on G3, CF, and CC.

This performance gap could be justified by two factors. On the one hand, graphite resistivity is about 200 times lower than those of felt and cloth (González-García et al., 1999). This possibly led to more EA bacteria, especially the *Geobacteraceae* family, colonizing the electrode and greater current density obtained with G3 graphite. To our knowledge, the direct correlation between extracellular electron transfer (EET) efficiency and support material electrical resistivity has yet to be demonstrated. This is mainly because producing materials with different resistivities but otherwise identical characteristics is challenging. Nevertheless, many studies have stated that a low electrical resistivity for the support material is necessary to obtain high current densities from bioanodes (Yu et al., 2017; Zhang et al., 2018).

3D pictures of EA biofilms revealed that anchoring to the surface seemed to be constituted of dispersed “pillars,” the whole biofilm not being in direct contact with the electrode (Erable and Bergel, 2009). It has also been suggested that EA biofilm formed with *Geobacter sulfurreducens* transfer electrons to the electrode not uniformly through the whole surface area but through patches where pioneering adherent cells play the role of “electrochemical gate” between the biofilm and the electrode surface (Dumas et al., 2008). Pons et al. (2011) stated that extremely high current densities (up to 280 A/m<sup>2</sup>) could be achieved locally in EA biofilms, especially with isolated bacteria and small colonies, when dense microbial colonies provided lower current densities. All these observations converge toward an electron transfer model that relies on the passage of high local current density through small patches rather than the passage of the average current density through the entire surface. Those high current points are the main EET zones, which means a large quantity of electrons is transferred through a small surface area. In such a context, the resistivity of the electrode could be a major rate-limiting cause because the higher is the local current, the higher is the potential drop opposed to the current.

On the other hand, CF and CC have hydrophobic surfaces (water contact angles, respectively 120 and 110°; Wang et al., 2007; Guo et al., 2014) while G3 graphite has a strongly hydrophilic surface (contact angle 50°). As discussed in section Electrical Resistivity, hydrophilic surfaces are beneficial for EA biofilms and the current density differences observed between CF, CC, and G3 graphite might also be linked to the significant difference between their hydrophilic properties.

## CONCLUSION

Even if the five grades of graphite tested all had close properties in term of electrical resistivity, surface roughness and hydrophobicity, the grade of the synthetic graphite really makes a strong impact on the current densities obtained. Among the graphite grades tested, G3 produced the highest steady state current (2.3 A/m<sup>2</sup>), giving it the best performance/mechanical strength/price ratio of all the graphite grades tested. The

differences exist, they are self-evident. But the reasons why one grade more than another is able to initiate the formation of a high-performance bioanode are still unclear and are undoubtedly conditioned by the elaboration protocols of synthetic graphite grades. The main fact to keep in mind is that the grade of graphite is something significantly impacting and that we can no longer talk about a synthetic graphite electrode as a common, universally comparable material. The predictions or observations made today on the basis of graphite bioanodes cannot be generalized to all graphite electrodes. Even at this detailed stage of graphite grade, the use of an electrode material and its comparison with another material inevitably requires experimental tests.

Steady state current density obtained with G3 was 50% higher than with CF and CC, which are commonly used 3D carbon materials for bioanodes. Bacterial communities and surface colonization were roughly similar on the G3 graphite grade, CF and CC, with a high enrichment in EA bacteria of the genus *Geobacter* even more important on G3. The electrical resistivity of G3, 200 times lower than those of CC and CF plus its strongly hydrophilic surface, could explain an intensification of the EET within the biofilm and the improved current densities obtained with G3. The influence of anode material resistivity on EA bacterial communities, EET mechanisms, and the physical structure of biofilms on electrodes will be an interesting research path for the future, especially considering very intense local electrons flow (current) as discussed with the example of “electron transfer gates.”

For the future, the standardized bio-electrochemical test protocol described in this study for the anodic materials comparison can be greatly useful to benchmark other materials as potential efficient dWW-fed bioanode support materials.

## DATA AVAILABILITY STATEMENT

The datasets generated for this study are available on request to the corresponding author.

## AUTHOR CONTRIBUTIONS

ER, AB, RB, and BE: study design and article writing. ER and LE: experiments. ER, RL, SD, LE, AB, RB, and BE: data analysis.

## FUNDING

This work was funded by the French ANR within the framework of the WE-MET project (ERANETMED 2015 European call).

## SUPPLEMENTARY MATERIAL

The Supplementary Material for this article can be found online at: <https://www.frontiersin.org/articles/10.3389/fenrg.2019.00106/full#supplementary-material>

## REFERENCES

- Aiken, D. C., Curtis, T. P., and Heidrich, E. S. (2019). Avenues to the financial viability of microbial electrolysis cells [MEC] for domestic wastewater treatment and hydrogen production. *Int. J. Hydrogen Energy* 44, 2426–2434. doi: 10.1016/j.ijhydene.2018.12.029
- Barker, D. J., Mannucci, G. A., Salvi, S. M. L., and Stuckey, D. C. (1999). Characterisation of soluble residual chemical oxygen demand (COD) in anaerobic wastewater treatment effluents. *Water Res.* 33, 2499–2510. doi: 10.1016/S0043-1354(98)00489-8
- Baudler, A., Schmidt, I., Langner, M., Greiner, A., and Schröder, U. (2015). Does it have to be carbon? Metal anodes in microbial fuel cells and related bioelectrochemical systems. *Energy Environ. Sci.* 8, 2048–2055. doi: 10.1039/C5EE00866B
- Blanchet, E., Desmond-Le Quemener, E., Erable, B., Bridier, A., Bouchez, T., and Bergel, A. (2015). Comparison of synthetic medium and wastewater used as dilution medium to design scalable microbial anodes: application to food waste treatment. *Bioresour. Technol.* 185, 106–115. doi: 10.1016/j.biortech.2015.02.097
- Blanchet, E., Erable, B., De Solan, M. L., and Bergel, A. (2016). Two-dimensional carbon cloth and three-dimensional carbon felt perform similarly to form bioanode fed with food waste. *Electrochem. Commun.* 66, 38–41. doi: 10.1016/j.elecom.2016.02.017
- Bond, D. R., Holmes, D. E., Tender, L. M., and Lovley, D. R. (2002). Electrode-reducing microorganisms that harvest from marine sediments. *Science* 295, 483–485. doi: 10.1126/science.1066771
- Bridier, A., Desmond-Le Quemener, E., Bureau, C., Champigneux, P., Renvoise, L., Audic, J. M., et al. (2015). Successive bioanode regenerations to maintain efficient current production from biowaste. *Bioelectrochemistry* 106, 133–140. doi: 10.1016/j.bioelechem.2015.05.007
- Cercado-Quezada, B., Byrne, N., Bertrand, M., Pocaznoi, D., Rimboud, M., Achouak, W., et al. (2013). Garden compost inoculum leads to microbial bioanodes with potential-independent characteristics. *Bioresour. Technol.* 134, 276–284. doi: 10.1016/j.biortech.2013.01.123
- Champigneux, P., Delia, M. L., and Bergel, A. (2018). Impact of electrode micro- and nano-scale topography on the formation and performance of microbial electrodes. *Biosens. Bioelectron.* 118, 231–246. doi: 10.1016/j.bios.2018.06.059
- Characklis, W. G. (2009). Bioengineering report: fouling biofilm development: a process analysis. *Biotechnol. Bioeng.* 102, 309–347. doi: 10.1002/bit.22227
- Chong, P., Erable, B., and Bergel, A. (2019). Effect of pore size on the current produced by 3-dimensional porous microbial anodes: a critical review. *Bioresour. Technol.* 289:121641. doi: 10.1016/j.biortech.2019.121641
- Dumas, C., Basseguy, R., and Bergel, A. (2008). Electrochemical activity of *Geobacter sulfurreducens* biofilms on stainless steel anodes. *Electrochim. Acta* 53, 5235–5241. doi: 10.1016/j.electacta.2008.02.056
- Erable, B., and Bergel, A. (2009). First air-tolerant effective stainless steel microbial anode obtained from a natural marine biofilm. *Bioresour. Technol.* 100, 3302–3307. doi: 10.1016/j.biortech.2009.02.025
- Escapa, A., Gómez, X., Tartakovsky, B., and Morán, A. (2012). Estimating microbial electrolysis cell (MEC) investment costs in wastewater treatment plants: case study. *Int. J. Hydrogen Energy* 37, 18641–18653. doi: 10.1016/j.ijhydene.2012.09.157
- Flint, S. H., Brooks, J. D., and Bremer, P. J. (2000). Properties of the stainless steel substrate, influencing the adhesion of thermo-resistance Streptococci. *J. Food Eng.* 43, 235–242. doi: 10.1016/S0260-8774(99)00157-0
- Gil-Carrera, L., Escapa, A., Moreno, R., and Morán, A. (2013). Reduced energy consumption during low strength domestic wastewater treatment in a semi-pilot tubular microbial electrolysis cell. *J. Environ. Manage.* 122, 1–7. doi: 10.1016/j.jenvman.2013.03.001
- González-García, J., Bonete, P., Expósito, E., Montiel, V., Aldaz, A., and Torregrosa-Maciá, R. (1999). Characterization of a carbon felt electrode: structural and physical properties. *J. Mater. Chem.* 9, 419–426. doi: 10.1039/a805823g
- Gude, V. G. (2016). Wastewater treatment in microbial fuel cells - an overview. *J. Clean. Prod.* 122, 287–307. doi: 10.1016/j.jclepro.2016.02.022
- Guo, K., Freguia, S., Dennis, P. G., Chen, X., Donose, B. C., Keller, J., et al. (2013). Effects of surface charge and hydrophobicity on anodic biofilm formation, community composition, and current generation in bioelectrochemical systems. *Environ. Sci. Technol.* 47, 7563–7570. doi: 10.1021/es400901u
- Guo, K., Soeriyadi, A. H., Patil, S. A., PrévotEAU, A., Freguia, S., Gooding, J. J., et al. (2014). Surfactant treatment of carbon felt enhances anodic microbial electrocatalysis in bioelectrochemical systems. *Electrochem. Commun.* 39, 1–4. doi: 10.1016/j.elecom.2013.12.001
- Heidrich, E. S., Dolfing, J., Scott, K., Edwards, S. R., Jones, C., and Curtis, T. P. (2013). Production of hydrogen from domestic wastewater in a pilot-scale microbial electrolysis cell. *Appl. Microbiol. Biotechnol.* 97, 6979–6989. doi: 10.1007/s00253-012-4456-7
- Hou, Y., Zhang, R., Luo, H., Liu, G., Kim, Y., Yu, S., et al. (2015). Microbial electrolysis cell with spiral wound electrode for wastewater treatment and methane production. *Process Biochem.* 50, 1103–1109. doi: 10.1016/j.procbio.2015.04.001
- Kadier, A., Simayi, Y., Abdeshahian, P., Azman, N. F., Chandrasekhar, K., and Kalil, M. S. (2014). A comprehensive review of microbial electrolysis cells (MEC) reactor designs and configurations for sustainable hydrogen gas production. *Alexandria Eng. J.* 55, 427–443. doi: 10.1016/j.aej.2015.10.008
- Kano, T., Suito, E., Hishida, K., and Miki, N. (2012). Effect of microscale surface geometry of electrodes on performance of microbial fuel cells micromachined microbial and photosynthetic fuel cells. *Jpn. J. Appl. Phys.* 51, 6–4. doi: 10.7567/JJAP.51.06FK04
- Ketep, S. F., Bergel, A., Calmet, A., and Erable, B. (2014). Stainless steel foam increases the current produced by microbial bioanodes in bioelectrochemical systems. *Energy Environ. Sci.* 7, 1633–1637. doi: 10.1039/C3EE44114H
- Kitching, M., Butler, R., and Marsili, E. (2017). Microbial bioelectrosynthesis of hydrogen: current challenges and scale-up. *Enzyme Microb. Technol.* 96, 1–13. doi: 10.1016/j.enzmtec.2016.09.002
- Koch, C., and Harnisch, F. (2016). Is there a specific ecological niche for electroactive microorganisms? *ChemElectroChem* 3, 1282–1295. doi: 10.1002/celec.201600079
- Kumar, R., Singh, L., and Zularisam, A. W. (2016). Exoelectrogens: recent advances in molecular drivers involved in extracellular electron transfer and strategies used to improve it for microbial fuel cell applications. *Renew. Sustain. Energy Rev.* 56, 1322–1336. doi: 10.1016/j.rser.2015.12.029
- Liu, H., Hu, H., Chignell, J., and Fan, Y. (2010). Microbial electrolysis: novel technology for hydrogen production from biomass. *Biofuels* 1, 129–142. doi: 10.4155/bfs.09.9
- Liu, H., Ramnarayanan, R., and Logan, B. E. (2004). Production of electricity during wastewater treatment using a single chamber microbial fuel cell. *Environ. Sci. Technol.* 38, 2281–2285. doi: 10.1021/es034923g
- Mateo, S., Cañizares, P., Rodrigo, M. A., and Fernandez-Morales, F. J. (2018). Biofilm and planktonic population distribution. Key aspects in carbonaceous anodes for microbial fuel cells. *J. Chem. Technol. Biotechnol.* 93, 3436–3443. doi: 10.1002/jctb.5701
- Nam, J. Y., Yates, M. D., Zaybak, Z., and Logan, B. E. (2014). Examination of protein degradation in continuous flow, microbial electrolysis cells treating fermentation wastewater. *Bioresour. Technol.* 171, 182–186. doi: 10.1016/j.biortech.2014.08.065
- Pannell, T. C., Goud, R. K., Schell, D. J., and Borole, A. P. (2016). Effect of fed-batch vs. continuous mode of operation on microbial fuel cell performance treating biorefinery wastewater. *Biochem. Eng. J.* 116, 85–94. doi: 10.1016/j.bej.2016.04.029
- Peckner, D., and Bernstein, I. M. (1977). *Handbook of Stainless Steels*. New York, NY: McGraw Hill.
- Picioreanu, C., Van Loosdrecht, M. C. M., and Heijnen, J. J. (2001). Two-dimensional model of biofilm detachment caused by internal stress from liquid flow. *Biotechnol. Bioeng.* 72, 205–218. doi: 10.1002/1097-0290(20000120)72:2<205::AID-BIT9>3.0.CO;2-L
- Pocaznoi, D., Calmet, A., Etcheverry, L., Erable, B., and Bergel, A. (2012a). Stainless steel is a promising electrode material for anodes of microbial fuel cells. *Energy Environ. Sci.* 5:9645. doi: 10.1039/c2ee22429a
- Pocaznoi, D., Erable, B., Etcheverry, L., Delia, M.-L., and Bergel, A. (2012b). Forming microbial anodes under delayed polarisation modifies the electron transfer network and decreases the polarisation time required. *Bioresour. Technol.* 114, 334–341. doi: 10.1016/j.biortech.2012.03.042
- Pons, L., Délia, M. L., and Bergel, A. (2011). Effect of surface roughness, biofilm coverage and biofilm structure on the electrochemical efficiency of microbial cathodes. *Bioresour. Technol.* 102, 2678–2683. doi: 10.1016/j.biortech.2010.10.138

- Reguera, G., McCarthy, K. D., Mehta, T., Nicoll, J. S., Tuominen, M. T., and Lovley, D. R. (2005). Extracellular electron transfer via microbial nanowires. *Nature* 435, 1098–1101. doi: 10.1038/nature03661
- Roubaud, E., Lacroix, R., Da Silva, S., Bergel, A., Basséguy, R., and Erable, B. (2018). Catalysis of the hydrogen evolution reaction by hydrogen carbonate to decrease the voltage of microbial electrolysis cell fed with domestic wastewater. *Electrochim. Acta* 275, 32–39. doi: 10.1016/j.electacta.2018.04.135
- Santoro, C., Arbizzani, C., Erable, B., and Ieropoulos, I. (2017). Microbial fuel cells: from fundamentals to applications. A review. *J. Power Sources* 356, 225–244. doi: 10.1016/j.jpowsour.2017.03.109
- Santoro, C., Guilizzoni, M., Correa Baena, J. P., Pasaogullari, U., Casalegno, A., Li, B., et al. (2014). The effects of carbon electrode surface properties on bacteria attachment and start up time of microbial fuel cells. *Carbon N. Y.* 67, 128–139. doi: 10.1016/j.carbon.2013.09.071
- Wang, H., Wang, G., Ling, Y., Qian, F., Song, Y., Lu, X., et al. (2013). High power density microbial fuel cell with flexible 3D graphene-nickel foam as anode. *Nanoscale* 5, 10283–10290. doi: 10.1039/c3nr03487a
- Wang, Y., Wang, C. Y., and Chen, K. S. (2007). Elucidating differences between carbon paper and carbon cloth in polymer electrolyte fuel cells. *Electrochim. Acta* 52, 3965–3975. doi: 10.1016/j.electacta.2006.11.012
- Wei, J., Liang, P., and Huang, X. (2011). Recent progress in electrodes for microbial fuel cells. *Bioresour. Technol.* 102, 9335–9344. doi: 10.1016/j.biortech.2011.07.019
- Xie, X., Criddle, C., and Cui, Y. (2015). Design and fabrication of bioelectrodes for microbial bioelectrochemical systems. *Energy Environ. Sci.* 8, 3418–3441. doi: 10.1039/C5EE01862E
- Yu, Y. Y., Zhai, D. D., Si, R. W., Sun, J. Z., Liu, X., and Yong, Y. C. (2017). Three-dimensional electrodes for high-performance bioelectrochemical systems. *Int. J. Mol. Sci.* 18:E90. doi: 10.3390/ijms18010090
- Zhang, L., He, W., Yang, J., Sun, J., Li, H., Han, B., et al. (2018). Bread-derived 3D macroporous carbon foams as high performance free-standing anode in microbial fuel cells. *Biosens. Bioelectron.* 122, 217–223. doi: 10.1016/j.bios.2018.09.005
- Zhou, M., Chi, M., Luo, J., He, H., and Jin, T. (2011). An overview of electrode materials in microbial fuel cells. *J. Power Sources* 196, 4427–4435. doi: 10.1016/j.jpowsour.2011.01.012

**Conflict of Interest:** RL is employed as research engineer by company 6T-MIC. SD is CEO of company 6T-MIC.

The remaining authors declare that the research was conducted in the absence of any commercial or financial relationships that could be construed as a potential conflict of interest.

Copyright © 2019 Roubaud, Lacroix, Da Silva, Etcheverry, Bergel, Basséguy and Erable. This is an open-access article distributed under the terms of the Creative Commons Attribution License (CC BY). The use, distribution or reproduction in other forums is permitted, provided the original author(s) and the copyright owner(s) are credited and that the original publication in this journal is cited, in accordance with accepted academic practice. No use, distribution or reproduction is permitted which does not comply with these terms.